FULL PAPER

ADVANCED FUNCTIONAL MATERIALS

DOI: 10.1002/adfm.200600204

Controlled Encapsulation of Hydrophobic Liquids in Hydrophilic Polymer Nanofibers by Co-electrospinning**

By *Juan Esteban Díaz*, *Antonio Barrero*, *Manuel Márquez*, and *Ignacio G. Loscertales**

There are many technical situations, such as various biological or medical applications, in which a hydrophobic fluid must be encapsulated inside a hydrophilic polymer shell in the form of tiny microscopic pieces. A novel approach is presented, based on the co-electrospinning of the hydrophilic polymer melt (outside) and the hydrophobic fluid (inside), which results in beaded micro- and nanofibers, such that the hydrophobic fluid is efficiently encapsulated inside the beads. For the selected fluid couple, the low liquid–liquid surface tension and the high viscosity of the melt prevent the varicose break-up of inner fluid in the coaxial electrified jet until the very end of the co-electrospinning process. The resulting fibers present beads filled with the hydrophobic fluid, separated by a rather uniform distance whose length depends partially on the melt flow rate. The bead diameter grows with the inner flow rate, going from a monosized to a bisized distribution. In the case under study, the maximum relative (inner-to-outer) flow rate is one. The diameter of the solid fibers between beads scales well with existing theories for simple electrospinning.

1. Introduction

Encapsulation is a common approach for protecting substances of interest from harsh environments. Within this broad setting, there are situations in which it is important that the encapsulated material is divided into tiny quantities with characteristic sizes in the micro- or nanometer regime. Examples can be found in drug delivery, where, in order to survive and to overcome biological barriers, capsules carried in the bloodstream need to have diameters smaller than a certain threshold, typically below a few hundred nanometers. There are many different methods in which the final product consists of clusters of micro- or nanocapsules in the form of powder, or dispersed in the form of an emulsion.[1] There are situations, however, in which the labile material must exert its function in a known, predefined location, for example, in protective coatings, sensing, and filtering. In this framework, the encapsulated material should not be capable of free movement, but it should somehow be fixed to a certain spot. One way of doing so is by encapsulating the labile substance in fibers; the fibers can then be placed at the desired location, thus anchoring the labile material in place. If the fibers must be nanometric in diameter, an appropriate way of achieving this is by electrospinning. In the standard approach, the labile substance is dissolved in a polymer melt, and the complete mixture is electrospun.[2] The results are nanofibers with a rather homogeneous distribution of the labile substance. A different method was previously reported by Sanders et al.,[3] where they electrospun a hydrophobic polymer melt (poly(ethylene-*co*-vinyl acetate), PEVA, in dichloromethane) in which an aqueous protein solution was previously emulsified. The results were PEVA microfibers in which small, polydisperse pockets of the aqueous solution were radially and axially randomly distributed. From the materials science point of view, these types of fibers are attractive because their radial and axial anisotropy could be of use for different applications.

This framework of encapsulation has been broadened by the use of electrified coaxial micro- and nanojets for coaxial electrospinning, or co-electrospinning, of two different liquids.[4] This method allows one-step fabrication of micro- and nanotubes or coaxial micro- and nanofibers of different pairs of polymers for different applications.[5,6] These are all structures with radial anisotropies. Very recently, co-electrospinning has been used to encapsulate labile materials other than polymers within fibers. For instance, Song et al.[7] used a stabilized emulsion of FePt magnetic nanoparticles in hexane as the inner liquid, and a melt

[*] Prof. I. G. Loscertales
E.T.S. Ingenieros Industriales, Universidad de Malaga
Plaza El Ejido, s/n 29013 Malaga (Spain)
E-mail: loscertales@uma.es
J. E. Díaz
Yflow SL
Marie Curie 4-12, 29590 Campanillas, Malaga (Spain)
Prof. A. Barrero
Escuela Superior de Ingenieros, Universidad de Sevilla
Camino de los Descubrimientos, s/n, 41092 Sevilla (Spain)
Dr. M. Márquez
Harrington Department of Bioengineering, Arizona State University
Tempe, AZ 85287-9709 (USA)
Dr. M. Márquez
Research Center, Philip Morris USA,4201 Commerce Road
Richmond, VA 23234 (USA)

[**] We thank Mr. A. Gómez, from E. S. Ingenieros de Sevilla, Spain, for measuring the surface tension of the different liquids, and Ms. E. Rojo from University of Basque Country, Spain, for kindly helping us with the rheological characterization of the melts. Finally, we acknowledge Prof. Juan Fernández de la Mora for helping us to improve the experimental setup. We acknowledge the support of the Spanish Ministry of Science and Technology under projects DPI2004-05246-C04 and NAN2004-09312-C03, and of Yflow SL.

ADVANCED FUNCTIONAL MATERIALS

of poly(ε-caprolactone) (PCL) on the outside to encapsulate the nanoparticles inside nanofibers. Jiang et al.[8] used an aqueous melt of poly(ethylene oxide) (PEO) in which a protein (bovine serum albumin (BSA) and lysozyme) was dissolved as the inner fluid, with a melt of PCL on the outside. The result was coaxial nanofibers containing the protein in their core fiber.

However, there are many situations in which hydrophobic substances need to be encapsulated by hydrophilic polymers, still in the form of fibers. Examples can again be found in drug delivery or in cosmetics, among many others, where hydrophobic drugs need to be encapsulated in biocompatible (typically hydrophilic) materials to reach a sufficient concentration in blood, or to penetrate through skin. Co-electrospinning for encapsulation, however, has so far been used only with either pairs of polymer melts (including sol–gels as "polymers"), or with polymers and regular liquids miscible with the solvent of the melt. (N.B. Loscertales et al. and Li and Xia[5] used regular, non-structured, hydrophobic liquids as the interior fluids, however their aim was not to encapsulate them, but to use them as a template for generating nanotubes.) For instance, in the work of Song et al.,[7] the hexane (inner liquid) is miscible with chloroform, the dominant solvent of the PCL melt. The group of Wnek and co-workers,[3] however, used a hydrophobic melt to encapsulate a hydrophilic solution, previously emulsified in the melt, into fibers by single-cone electrospinning. To our knowledge, in any other cases both inner and outer fluids consist of polymer melts, with or without labile materials.

In this work we use co-electrospinning of a hydrophilic polymer melt as the outer fluid and a hydrophobic regular liquid (non-polymeric) as the inner fluid for fiber encapsulation. The resulting fibers present beads filled with the hydrophobic liquid regularly distributed along the fibers. The size of the beads is rather uniform, although may become bimodal depending on the operating conditions. Both bead size and bead-to-bead separation distance can be (mainly) controlled within a certain range by adjusting the flow rates of both fluids through the spinneret. Aside from encapsulation, this process could also be useful for producing fibers with controlled axial anisotropies (composition) in the micrometer and sub-micrometer regime.

2. Results and Discussion

A photograph of a compound poly(vinyl pyrrolidone) (PVP)–oil Taylor cone is shown in Figure 1. The outer liquid is the PVP melt and the inner liquid is the oil. The flow rates are 0.4 and 0.04 mL h^{-1}, respectively. The establishment of such a compound cone requires that the fluids exhibit certain characteristics. A sufficiently high viscosity of the outer fluid together with a low value of the oil/melt interfacial tension is essential to develop a compound cone in steady state. Otherwise, for large values of the interfacial tension or low viscosity, the viscous drag exerted by the melt on the oil's surface is unable to overcome the cohesive force of the surface tension, so the inner meniscus (oil) remains quasispherical and no double cone is developed. In some situations, the inner meniscus reaches the region where the cone deforms into a jet; at that point, the spherical inner meniscus may develop a tiny cusp that emits a finite number of small droplets to finally recoil to a quasi-spherical shape (i.e., unsteady tip streaming). This unsteady process may repeat itself cyclically. In general, by lowering the oil/melt interfacial tension, the inner meniscus can be steadily pulled into a jet by the outer melt. This can be achieved by adding suitable surfactants, although it was not necessary in our particular case. In the reported experiments, the fibers were generated under conditions such that both the emitted current and the compound cone appear to be in steady state.

Figure 1. Compound Taylor cone. Outer fluid: PVP–DMF (DMF: dimethyl formamide) melt. Inner liquid: oil. Inner needle outer diameter (OD) is 0.5 mm.

Apart from the requirements regarding the physical properties of the fluids, for a given setup and fluid pair there exists a parametrical range of operation in which the compound cone and so the compound fibers are produced. For a fixed voltage difference between the spinneret and the collector, the operative range depends on the flow rates of both fluids. We have found a range, without in depth exploration of the limits, in which we can easily operate. Typically, the inner fluid flow rate, Q_{in}, may be set at K times the outer fluid flow rate, Q_{out}. K varies roughly between 1 and 0.1 in our case. Q_{out} varies between 0.1 and 1 mL h^{-1}. Figure 2 shows qualitatively how the compound cone develops as K increases from 0.1 for $Q_{out} = 0.4$ mL h^{-1}. As K grows, the compound meniscus grows (Fig. 2a and b) until the flow inside the meniscus starts mixing both fluids ($K \approx 1$, Fig. 2c); in such a case, although fibers are still generated, they appear to be wet due to the presence of oil (non-volatile) on the fiber surface, see Figure 2d. This indicates that the encapsulation process has broken down due to the mixing occurring within the cone. For other values of Q_{out}, the phenomenology as K varies is similar.

To demonstrate encapsulation we chose to use special markers that are regularly added to industrial oils to identify leaks, which fluoresce when irradiated by UV light. PVP nanofibers that are dry at room conditions do not emit under UV light.

Figure 3 shows an example of the as-collected fibers when a steady-state compound cone/jet is run. In this case, $Q_{out} = 0.4$ mL h^{-1} and $Q_{in} = 0.02$ mL h^{-1}. A noticeable difference in the resulting fibers when compared with regular PVP fibers made from the same melt is the presence of beads. When the mat is irradiated with UV light, only the beads fluoresce, indicating to us that the oil is confined or encapsulated solely

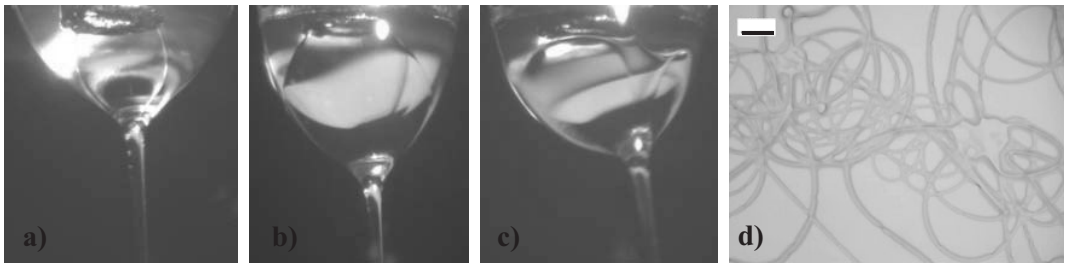

Figure 2. Evolution of PVP–oil Taylor cone geometry. Outer and inner flow rates are: a) 0.4–0.04 mL h^{-1}; b) 0.4–0.2 mL h^{-1}; c) 0.4–0.5 mL h^{-1}. Inner needle OD is 0.5 mm. d) Oil covered microfibers as a result of $Q_{out}/Q_{in} \approx 1$. Scale bar: 20 μm.

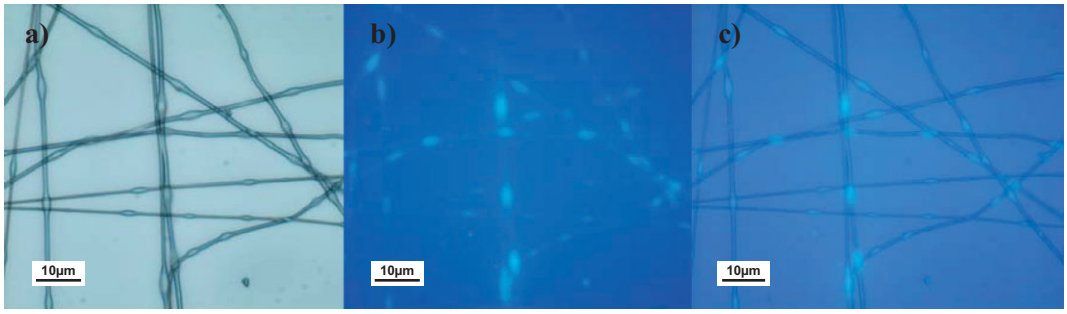

Figure 3. Optical images of PVP–oil fibers. Excitation and emission light are: a) visible light; b) UV light ($\lambda_{ex} = 330$–380 nm, $\lambda_{em} = 420$ nm) and c) both photographs, overlapped. Oil located at bright spots. Scale bars are 10 μm.

inside these beads (Fig. 3b and c). It should be noted that the mat has not been washed or flushed with solvents, so that the absence of fluorescence everywhere apart from the beads confirms that the oil is efficiently encapsulated inside the beads.

A closer look at the structure of the beads may be achieved by crosslinking the PVP. When the nonwoven mats are heated at 200 °C in ambient air for 4 h, the PVP oxidizes and crosslinks.[9] Thus, the polymeric shell becomes rigid, preserving the shape of both the fibers and the beads. This "rigid" mat can be mechanically broken[10] to analyze the inner structure of both fibers and beads by scanning electron microscopy (SEM). Such analysis is shown in Figure 4. As-collected nanofibers that have not undergone thermal treatment are shown in Figure 4a. After the thermal treatment, the mat is broken; Figure 4b shows the hollow structure of the beads while Figure 4c shows the solid nanofibers between beads. This analysis further supports the theory that the oil is encapsulated solely inside the beads.

Accordingly, although a steady compound cone (and coaxial jet) is set up, the final fibers are such that the inner oil does not form a continuous core, but a string of discrete pockets. This indicates that the inner jet (oil), which is a Newtonian liquid, undergoes varicose break up at a faster rate than the solidification of the outer melt happens, even though the small interfacial tension and the high viscosity of the outer liquid slow down the break-up process.

Below we present the evolution of the measured fiber and bead diameters, bead-to-bead distance, and emitted current as a function of liquid flow rates. Let us recall that both the spinneret-to-collector distance and the voltage are kept practically constant in all the experiments.

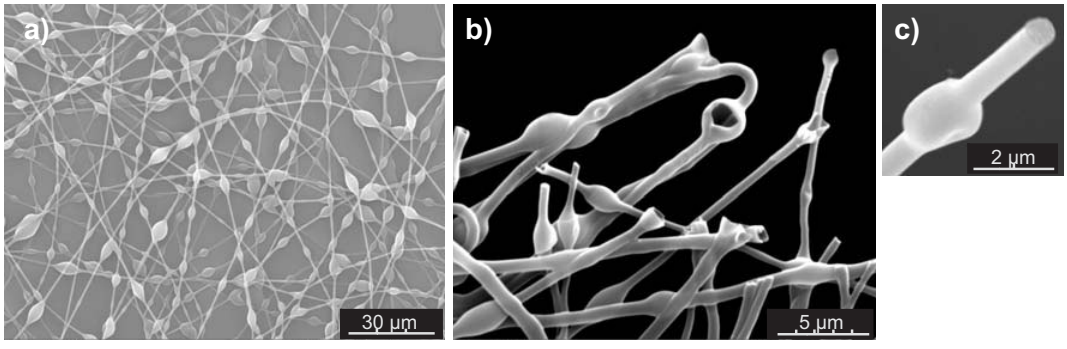

Figure 4. Scanning electron microscopy (SEM) images of PVP–oil nanofibers: a) beads on fibers as-collected; b) view of the hollow structure of the beads, and c) detail of the solid fibers between beads.

ADVANCED FUNCTIONAL MATERIALS

Figure 5 collects the measurements of the emitted current I versus Q_{out}. The values of I varied at most by ±2 nA. Each data point corresponds to a given value of Q_{in}. I behaves almost linearly with Q_{out}, while being independent of Q_{in}. The null role of Q_{in} might be qualitatively understood by the much lower conductivity of the oil (4.35×10^{-7} S m^{-1}) compared to that of the melt (1.34×10^{-3} S m^{-1}), together with its modest flow rate ($0.1 \leq K \leq 1$): its rather high dielectric character may seldom help to drive current by conduction.

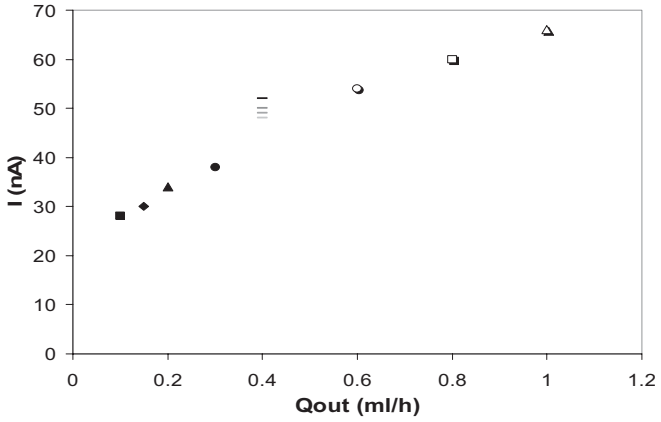

Figure 5. Current I (nA) versus outer flow rate Q_{out} (mL h^{-1}). Inner flow rates Q_{in} (mL h^{-1}) are ■: 0.02; ◆: 0.02; ▲: 0.02; ●; 0.02; light-gray dash: 0.02–0.04–0.06–0.08–0.1–0.15–0.2; mid-gray dash: 0.25; dark-gray dash: 0.3; black dash: 0.35–0.4–0.5; ○ 0.02–0.04; □ 0.04–0.06, and △ 0.1. Current fluctuations are ±2nA at most.

Figure 6 presents various size measurements. Figure 6a and b shows the fiber diameter, D, and the center of the bead-to-center of the bead fiber length, L, as a function of Q_{out}, respectively. Figure 6c shows the bead diameters D_b as a function of Q_{in} for a fixed value of $Q_{out} = 0.4$ mL h^{-1}. Each data point in these figures is the average value of at least 30 measurements on optical microscopy images. The errors in the measurement procedure are within 100 nm. The vertical lines shown in Figure 6a–c represent the standard deviation (s.d.) associated with each data point. As shown in Figure 6a and b, both D and L exhibit a trend that seems to increase with Q_{out}, although very slowly. While D remains independent of Q_{in}, L decreases as Q_{in} increases (not shown), although $|\partial L/\partial Q_{in}| = A\,\partial L/\partial Q_{out}$, where $A \sim 1/2$ or 1/3, so that Q_{out} remains the dominant controlling parameter for L.

On the other hand, the bead diameter D_b does depend on Q_{in}, and is independent of Q_{out}. Another feature shown in Figure 6c is the transition from a monomodal to a bimodal bead size distribution for Q_{in} values larger than 0.08 mL h^{-1}. The dashed lines are the linear regression of data points of each mode. The appearance of smaller beads (Fig. 6d) resembles the typical satellite droplets formed when a viscous liquid jet breaks up, as reported by Oliveira and McKinley[11] The diameter of the larger beads grows with Q_{in} faster than that of the smaller beads. Figure 7 shows examples of the evolution of the bead distribution as the inner flow rate increases.

Regarding the fate of the inner jet, if its break up occurred at early stages of the spinning process, the first generation of offspring oil droplets would move apart from each other and would also be elongated as the stretching proceeds. Eventually,

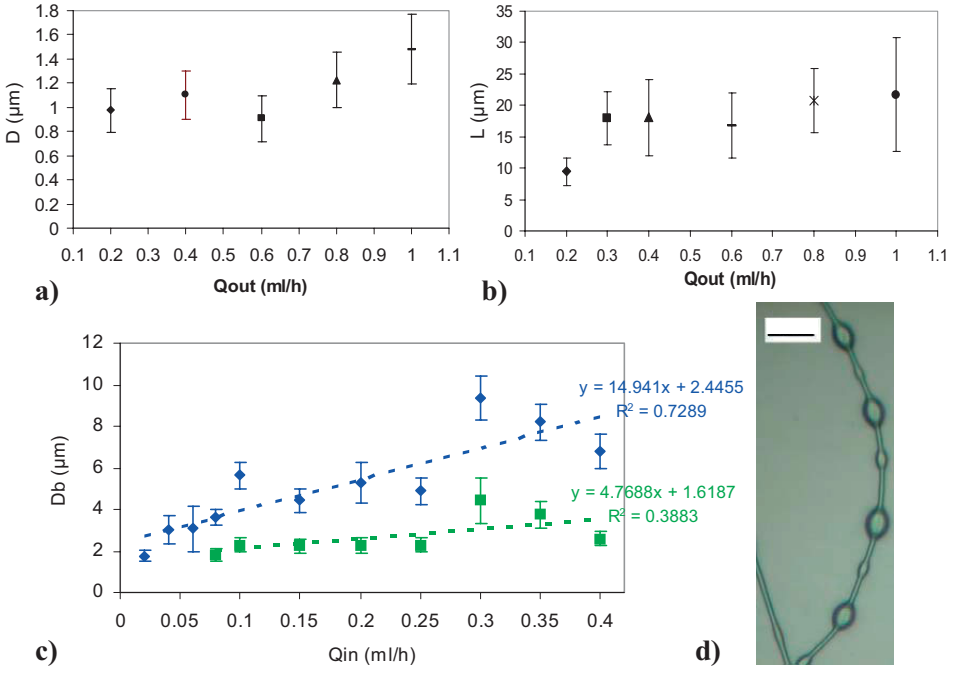

Figure 6. a) Fiber diameter, D, and b) average center-to-center distance between beads, L, both as a function of Q_{out}. Segments represent the standard deviation (s.d.). c) Plot showing the appearance of smaller (satellite) beads (green squares) along with larger beads (blue diamonds) depending on Q_{in}, fixed $Q_{out} = 0.4$ mL h^{-1}. Dashed lines are their linear regression trends. d) Image of satellite and principal beads on a fiber. Scale bar is 10 μm.

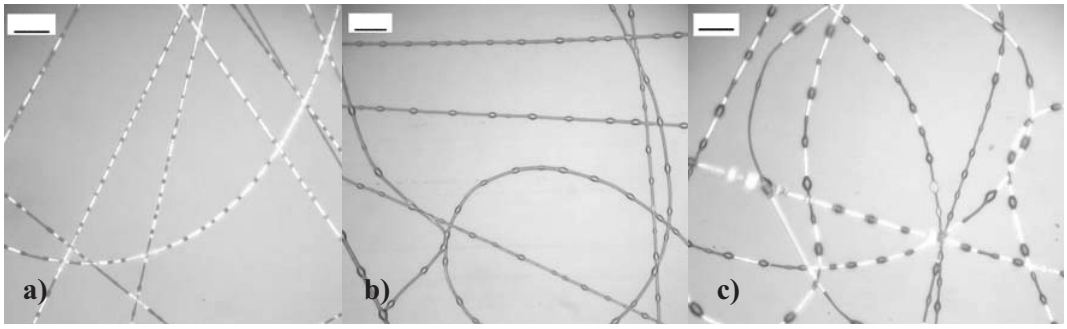

Figure 7. Monomodal bead-to-bead distances and incremental bead size photographs. Oil flow rates are: a) 0.02 ($K=10^{-1}$); b) 0.04 ($K=10^{-1}$); c) 0.25 mL h^{-1} ($K=0.6$). Scale bars are 20 μm.

each of these well-separated masses of oil would be stretched to the point where they break up into a second generation of (smaller) offspring. This process would lead to a bimodal distribution of the bead-to-bead distance, L: a small L_2 between consecutive droplets of the second generation, and a large L_1 associated with the relative separation undergone by the first generation of droplets before they break up. If further break up occurs (third and subsequent droplet generations), the distribution of L would be multimodal. The experiments, however, show that L is monomodal, with rather small size dispersion, indicating that the inner jet breaks up only once,[12] and that this happens in the final stages of the stretching.

Further support of this scenario might be obtained from the following crude mass balance. Just before the break up of the inner jet, let us assume that both fluids travel at the same velocity in the form of a coaxial jet with inner and outer diameters d_i and d_o, respectively. If λ is the axial break-up wavelength, one may assume that all the oil contained in the cylinder of length λ and diameter d_i will form the final oil bead of diameter D_b. Similarly, one may assume that all the mass of melt contained in the hollow cylinder with inner and outer diameters d_i and d_o, respectively, and length λ will form a fiber of length L and diameter D between two neighboring beads, since L is much larger than D_b. Using the experimental values of D_b and L, upon eliminating λ one obtains the experimental diameter ratio of the coaxial jet at the break-up point, $(d_o/d_i)_{exp}$. The ratio d_o/d_i of the coaxial jet may also be estimated from the liquid flow rates, $d_o/d_i=(Q_{out}/Q_{in}+1)^{1/2}$, which is a known constant assuming there is no solvent evaporation. The comparison between the two estimates yield $(d_o/d_i)_{exp}\approx 0.5(d_o/d_i)$, indicating that most of the volume of the melt is already removed by evaporation (of the order of 90 %) when the inner jet breaks up.

We have also compared the fiber diameter, D, with the scaling proposed by Fridrikh et al.,[13] in which a charged liquid jet is stretched under the whipping instability until its diameter reaches a minimum, D^*, at which the destabilizing electric stress on its surface is balanced by the stabilizing cohesive forces of the surface tension of the whipping ends. Their dynamic model leads to $D_F^*\approx\sum(\varepsilon_o\gamma)^{1/3}(Q/I)^{2/3}$, where Q is the melt flow rate, ε_o the permittivity of vacuum, γ the surface tension coefficient, and I the current transported by the jet. The parameter $\sum$ includes the effect of the setup geometry, the wavelength of the whipping instability, and the solvent evaporation; in our case it takes the value $\sum\approx 0.2093$ (According to Fridrikh et al.,[13] $\sum=C^{1/2}(2/\pi(2\ln\chi-3))^{1/3}$, where C is the polymer concentration and $\chi\sim R/h$ is the dimensionless wavelength of the instability responsible for the normal displacements. h is the jet diameter at the onset of instability and R the radius of curvature. They use $\chi=100$, although the exact value is not critical, since $\ln\chi$ varies slowly). From an static point of view, the maximum stretching of an infinitely long electrified cylindrical jet of a conducting liquid in air is reached when the electric pressure and surface tension balance each other, $1/2\sigma^2/\varepsilon_o\approx 2\gamma/D^*$, where σ is the surface charge density on the jet. The relation above, written in terms of known quantities, leads to $D^*\approx 4(\varepsilon_o\gamma)^{1/3}(Q/I)^{2/3}$, very similar to D_F^* except for the constant. To include the solvent evaporation in this latter expression, one must assume that 90 % of the melt volume is gone, consistent with the mass balance above. Thus, one might use $Q\approx 0.1\,Q_{out}$ and the experimental value of I plotted in Figure 5 to estimate D^*; since the oil mass is strictly contained in the beads, Q_{in} should not play a role in this case. Both predictions, D_F^* and D^*, are plotted versus Q_{out} in Figure 8 along with the experimental fiber diameters D. Interestingly, D^* re-

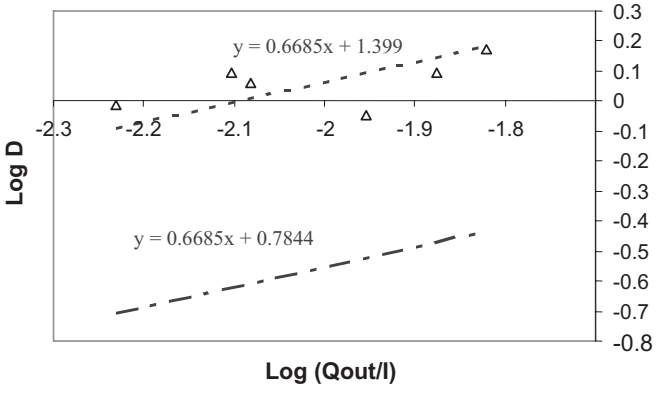

Figure 8. The log of experimental (D △), modeled in [12] (D_F*dot–dashed line) and our simplified model (D*dashed line) fiber diameters versus the inverse of volume charge density. Solid lines are the model linear regression trends.

ADVANCED FUNCTIONAL MATERIALS

produces the measured values better than D_F*, which turns out to underestimate the measured values by a factor of four. It is possible that the geometric differences between our setup and the one by Fridrikh et al.[13] are responsible for such differences, in which case the effect of the geometry on the final diameter must be investigated further. Nevertheless, either approach provides a method for predicting the fiber diameter between beads.

3. Conclusions

In this work we describe a utilization of electrified coaxial jets for encapsulating hydrophobic liquids in hydrophilic polymer melts, a product that would have applications in various technological fields, such as drug delivery. The process, in which a coaxial jet of polymer (outside) and a hydrophobic liquid (inner) is electrospun, produces beaded fibers, encapsulating the hydrophobic liquid into these beads. The beads are regularly distributed along the fibers, and their size exhibits a mono- or bimodal distribution, depending on the operating conditions (mainly the inner liquid flow rate). Both the bead-to-bead distance and fiber diameter may be controlled by the outer liquid flow rate, while the bead diameter may be controlled by adjusting the inner liquid flow rate. Although accurate prediction of the bead diameter and the bead-to-bead separation is still pending, the scaling of the fiber diameter for regular electrospinning seems to be appropriate in this case. The data shown above corresponds to a given melt–oil pair, although the process has also been successfully used with other fluid pairs (e.g., PEO and octanol, PEO and sunflower oil (Fig. 9), PEO and hexane, etc.). This implementation might also be useful for producing micro- and nanofibers with controlled distributions of axial anisotropies in composition. Note finally that the same scheme might be employed to encapsulate hydrophilic liquids inside nanofibers of hydrophobic polymers.

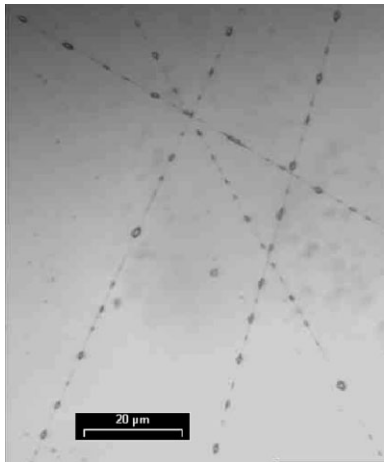

Figure 9. Sunflower oil encapsulated by PEO. Scale bar is 20 µm.

4. Experimental

Materials: We chose a biocompatible polymer to form the melt: poly(vinyl pyrrolidone) (PVP). The PVP (Acros Organics, weight-average molecular weight, $M_w = 1\,300\,000$) is dissolved in DMF (*N*,*N*-dimethylformamide) (Scharlau, reagent grade) by heating at 50 °C and stirring the solution for 24 h. Other solvents such water and ethanol can also be used for the PVP melt. We used a concentration of 20 wt % for PVP in DMF, which turned out to be the minimum concentration for electrospinning bead-free nanofibers. Its rheological behavior was characterized with a rheometer (Haake, RheoStress 600 AT instruments, ARG2). The viscosity at zero shear is 2600 cps (1 cps = $1 \times 10^{<M-3>}$ Pa s) at 25 °C. The electric conductivity of the PVP–DMF melt is 1.34×10^{-3} S m^{-1} at 25 °C. It was measured by filling a Teflon tubing of known length and inner diameter with the melt; by reading the electric current flowing through the tubing when a known voltage difference is applied between the ends, the conductivity is obtained.

The inner fluid is an industrial oil (SAE-15W50, Elf) used as purchased, which turns out to be fluorescent under UV light. (This type of oil also fluoresces under visible light, although the scattered light fades away in rather short periods of time.) The oil has a viscosity of 280 cps and a conductivity of 4.35×10^{-7} S m^{-1} at 25 °C. The surface tensions of DMF–air, melt–air, and oil–air at 25 °C are 29.5, 36.29, and 30.1 mN m^{-1}, respectively. The DMF/oil and the melt/oil interfacial tensions are 1.91 and 0.38 mN m^{-1}, respectively. The measurements were carried out with a pendant drop tensiometer (KSV, CAM-100).

Setup: The setup for coaxial electrospinning is depicted in Figure 10. In brief, the spinneret consists of two stainless-steel tubes, with outer diameters (ODs) 1.5 and 0.5 mm, and inner diameters (IDs) 1.1 and 0.39 mm, respectively. The tubes are placed coaxially, with the inner one sticking out slightly, just enough to visualize the compound meniscus. The collector, a rounded thin plate made of aluminum with a diameter of 25 cm, is axially located in front of the spinneret at about 30 cm. Two high-voltage power supplies are used (Gamma High Voltage, ES30P and Bertan, 205B-10R). The first one is connected to the spinneret, and raises its potential up to some +7 to +8 kV with respect to ground; the second one is connected to the collector, and lowers its potential down to –9 kV with respect to ground. Thus, the total voltage difference between the spinneret and the collector is typically between +16 and +17 kV.

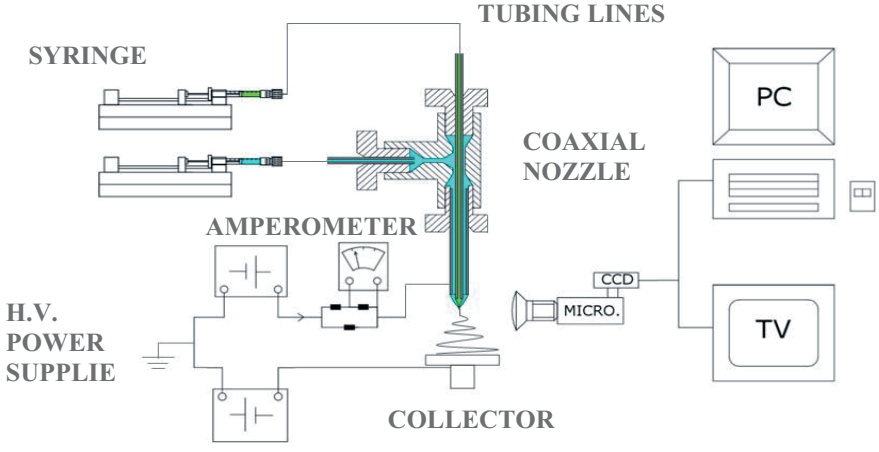

Figure 10. Sketch of the co-electrospinning setup.

The reason for using two power supplies is to reduce the voltage difference between the coaxial liquid jet and the grounded surroundings, to ensure that almost every fiber lands on the collector. These voltages and distances were selected simply because, for the materials and flow rates used, the fibers reached the collector dry enough to be manipulated afterwards. An optical microscope (Nikon, SMZ800) equipped with a camera (Nikon, Coolpix 4500) hooked to a computer allows visualization and recording of the compound meniscus at the spinneret exit. The liquid flow rates are independently imposed by two syringe pumps (Cole Parmer 74900 Series). The syringes used are Becton&Dickinson of 5 and 2 cm^3, made of Teflon. The current emitted from the spinneret was measured by inserting a floating voltmeter between the high voltage supply and the spinneret.

The current flowing through the voltmeter inner resistance (1 MΩ) provokes a voltage drop across it that is shown on the voltmeter screen; after calibration, the voltage on the screen can be translated to current.

Scanning electron microscopy (SEM) of the electrospun samples was performed on a JEOL JSM-840 JE (JEOL Ltd.) electron microscope. The fibers were gold-coated by sputtering (JEOL, JCC-1100) prior to examination.

Nonwoven mats were examined to verify oil encapsulation with an optical microscope (Nikon Eclipse, 800) in an excitation wavelength, λ_{ex}, between 330 and 380 nm and reception wavelength, λ_{em}, higher than 420 nm.

Received: March 2, 2006
Final version: April 27, 2006
Published online: September 19, 2006

[1] a) A. S. Utada, E. Lorenceau, D. R. Link, P. D. Kaplan, H. A. Stone, D. A. Weitz, *Science* **2005**, *308*, 537. b) A. G. Marín, A. Barrero, I. G. Loscertales, presented at 2005 APS division of fluid dynamics 58th Annual Meeting, Chicago, Nov. 20–22, 2005. c) B. G. Amsden, M. F. A. Goosen, *J. Controlled Release* **1997**, *43*, 183. d) R. Bocanegra, A. G. Gaonkar, A. Barrero, I. G. Loscertales, D. Pechack, M. Marquez, *J. Food Sci.* **2005**, *70*, 492.

[2] a) J. Xia, Y. Hsieh, *J. Mater. Sci.* **2003**, *38*, 2125. b) S. Lee, A. M. Belcher, *Nano Lett.* **2004**, *4*, 387. c) N. Tomczak, N. F. van Hulst, G. J. Vancso, *Macromolecules* **2005**, *38*, 7863.

[3] a) E. H. Sanders, R. Kloefkorn, G. L. Bowlin, D. G. Simpson, G. E. Wnek, *Macromolecules* **2003**, *36*, 3803. b) E. Kenawy, G. L. Bowlin, K. Mansfield, J. Layman, D. G. Simpson, E. H. Sanders, G. E. Wnek, *J. Controlled Release* **2002**, *81*, 57. c) G. Verreck, I. Chun, J. Peeters, J. Rosenblatt, M. E. Brewster, *Pharm. Res.* **2003**, *20*, 810.

[4] I. G. Loscertales, A. Barrero, I. Guerrero, R. Cortijo, M. Marquez, A. M. Gañan Calvo, *Science* **2002**, *295*, 1695.

[5] a) I. G. Loscertales, A. Barrero, M. Marquez, R. Spretz, R. Velarde-Ortiz, G. Larsen, *J. Am. Chem. Soc.* **2004**, *126*, 5376. b) D. Li, Y. Xia, *Nano Lett.* **2004**, *4*, 933.

[6] a) Z. Sun, E. Zussman, A. L. Yarin, J. H. Wendorff, A. Greiner, *Adv. Matter.* **2003**, *15*, 1929. b) J. H. Yu, S. V. Fridrikh, G. C. Rutledge, *Adv. Mater.* **2004**, *16*, 1562. c) J. E. Diaz, M. Lallave, D. Galan, M. Marquez, A. Barrero, I. G. Loscertales, presented at Fiber Society Spring 2005 Conf., St. Gallen, Switzerland, May 25–27, 2005.

[7] T. Song, Y. Zhang, T. Zhou, C. T. Lim, S. Ramakrishna, B. Liu, *Chem. Phys. Lett.* **2005**, *415*, 317.

[8] H. Jiang, Y. Hu, Y. Li, P. Zhao, K. Zhu, W. Chen, *J. Controlled Release* **2005**, *108*, 237.

[9] J. Scheirs, S. W. Bigger, E. T. H. Then, N. C. Billingham, *J. Polym. Sci., Part B* **1993**, *31*, 287.

[10] Regarding the mat break up, we suspect that during the heating process, the pressure in the core of the beads increases as the oil warms up until it eventually causes a brittle shield fracture through which the oil escapes. Nevertheless, there are other ways to crosslink PVP without the need for such high temperatures. See a) A. Charlesby, P. Alexander, *J. Polym. Sci.* **1955**, *23*, 355. b) H. K. Can, B. K. Denizli, S. Kavlak, A. Guner, *Radiat. Phys. Chem.* **2005**, *72*, 483.

[11] M. S. N. Oliveira, G. H. McKinley, *Phys. Fluids* **2005**, *17*, 071 704-1.

[12] Another possibility would be a continuous stretching-and-break-up process of the inner jet, but in such a special way that the final oil droplets are equally spaced along the fiber. The intrinsic non-uniformity of the whole spinning process prevents this from occurring.

[13] S. V. Fridrikh, J. H. Yu, M. P. Brenner, G. C. Rutledge, *Phys. Rev. Lett.* **2003**, *90*, 144 502-1.